

## New Polylactide/Layered Silicate Nanocomposites. 3. High-Performance Biodegradable Materials

Suprakas Sinha Ray,<sup>†</sup> Kazunobu Yamada,<sup>‡</sup> Masami Okamoto,<sup>\*,†</sup>  
Akinobu Ogami,<sup>‡</sup> and Kazue Ueda<sup>‡</sup>

Advanced Polymeric Materials Engineering, Graduate School of Engineering,  
Toyota Technological Institute, Hisakata 2-12-1, Tempaku, Nagoya 468 8511, Japan, and  
Unitika Ltd., Kojakura 23, Uji, Kyoto 611 0021, Japan

Received September 25, 2002. Revised Manuscript Received January 29, 2003

Our ongoing research on the preparation, characterization, materials properties, and biodegradability of polylactide (PLA)/organically modified layered silicate (OMLS) nanocomposites has yielded results for PLA/organically modified synthetic fluorine mica (OMSFM) nanocomposites. Synthetic fluorine mica (SFM), modified with *N*-(coco alkyl)-*N,N*-[bis(2-hydroxyethyl)-*N*-methylammonium cation, was used as an OMLS for the nanocomposites preparation. The internal structure of the nanocomposites in the nanometer range was established using wide-angle X-ray diffraction (WAXD) analyses and transmission electron micrographic (TEM) observations. All nanocomposites exhibited remarkable improvement of various materials properties with simultaneous improvement in biodegradability than that of neat PLA. This is the first report that deals with the ultimate degradability of PLA and corresponding nanocomposites under compost.

### Introduction

Advanced technology in petrochemical-based polymers has brought many benefits to mankind. However, it becomes more evident that the ecosystem is considerably disturbed and damaged as a result of the non-degradable plastic materials for disposable items. The environmental impact of persistent plastic wastes is increasing global concerns, and alternative disposal methods are limited. Incineration of the plastic wastes always produces a large amount of carbon dioxide and creates global warming, and sometimes produces toxic gases, which again contributes to global pollution. On the other hand, satisfactory landfill sites are also limited. Also, the petroleum resources are finite and becoming limited. For this reason there is an urgent need to develop renewable source-based environmental benign plastic materials, especially in short-term packaging and disposable applications that would not involve the use of toxic or noxious components in their manufacture and could allow composting to naturally occurring degradation products. Accordingly, polylactide (PLA) is of increasing commercial interest since it is completely made from renewable agricultural products with excellent properties comparable to many petroleum-based plastics and is readily biodegradable.<sup>1,2</sup> High-molecular-weight PLA is generally prepared by the ring-opening polymerization of lactide monomer,<sup>3,4</sup> which in turn is obtained from the fermentation of sugar feed-

stocks, corn, and so forth.<sup>5</sup> Even when burned, it produces no nitrogen oxide and only one-third the combustible heat generated by polyolefins, and it does not damage the incinerator and provides significant energy savings.<sup>6</sup>

Therefore, PLA is a promising polymer for various end-use applications,<sup>7</sup> and currently, there is increasing interest in using PLA for disposable and degradable plastic articles.<sup>8</sup> However, some of the other properties such as flexural properties, heat distortion temperature (HDT), gas permeability, impact factor, melt viscosity for further processing, and so forth, are frequently not good enough for various end-use applications.<sup>9</sup>

On the other hand, polymer/organically modified layered silicates (OMLS) nanocomposite technology has already proven to be a good way to improve these properties significantly.<sup>10–15</sup> In general, it is believed that these significant property improvements in nano-

(3) Kim, S. H.; Han, Y.-K.; Kim, Y. H.; Hong, S. I. *Macromol. Chem.* **1991**, *193*, 1623. Kricheldorf, H. R.; Serra, A. *Polym. Bull.* **1985**, *14*, 497. Kricheldorf, H. R.; Berl, M.; Scharngal, N. *Macromolecules* **1988**, *21*, 286.

(4) Nijenhuis, A. J.; Grijpma, D. W.; Pennings, A. J. *Macromolecules* **1992**, *25*, 6419.

(5) Lunt, J. *Polym. Degrad. Stab.* **1998**, *59*, 145.

(6) From Kanebo Ltd., Japan, wave site www.kanebotx.com (accessed Aug 27, 2002).

(7) Fang, Q.; Hanna, M. A. *Ind. Crops Prod.* **1999**, *10*, 47.

(8) Gu, J.-D.; Gada, M.; Kharas, G.; Eberiel, D.; McCarthy, S. P.; Gross, R. A. *Polym. Mater. Sci. Eng.* **1992**, *67*, 351.

(9) Ogata, N.; Jimenez, G.; Kawai, H.; Ogihara, T. *J. Polym. Sci., Part B: Polym. Phys.* **1997**, *35*, 389.

(10) LeBaron, P. C.; Wang, Z.; Pinnavaia, T. J. *J. Appl. Clay. Sci.* **1999**, *15*, 11.

(11) Alexander, M.; Dubois, P. *Mater. Sci. Eng., R.* **2000**, *28*, 1.

(12) Giannelis, E. P.; Krishnamoorti, R.; Manias, E. *Adv. Polym. Sci.* **1999**, *138*, 107.

(13) Biswas, M.; Sinha Ray, S. *Adv. Polym. Sci.* **2001**, *155*, 167.

(14) Giannelis, E. P. *Adv. Mater.* **1996**, *8*, 29.

(15) Usuki, A.; Kawasumi, M.; Kojima, Y.; Okada, A.; Kurauchi, T.; Kamiigaito, O. *J. Mater. Res.* **1993**, *8*, 1174.

\* To whom correspondence should be addressed. Tel.: +81 52 809 1861. Fax: +81 52 809 1864. E-mail: okamoto@toyota-ti.ac.jp.

<sup>†</sup> Toyota Technological Institute.

<sup>‡</sup> Unitika Ltd.

(1) Drumright, R. E.; Gruber, P. R.; Henton, D. E. *Adv. Mater.* **2000**, *12*, 1841.

(2) Martin, O.; Averous, L. *Polymer* **2001**, *42*, 6209. Tsuji, H.; Ikada, Y. *J. Appl. Polym. Sci.* **1998**, *67*, 405.

composites come from interfacial interactions between the polymer matrix and OMLS as opposed to conventional composites. The layered silicates have layer thickness on the order of 1 nm and very high aspect ratios (e.g., 10–1000). A few weight percent of OMLS, which is properly dispersed throughout the polymer matrix, thus creates much more surface area for polymer/filler interaction than do conventional composites.<sup>16</sup>

In our previous publications,<sup>17–19</sup> we reported on the preparation, characterization, and materials properties of PLA/montmorillonite (mmt) (modified either with octadecylammonium cation or trimethyl octadecylammonium cation) nanocomposites. The mechanical and practical materials properties of neat PLA (both in solid and molten states) were significantly improved by the introduction and intercalation of mmt, using a melt intercalation technique.

The main objective of this report is to describe the preparation, characterization, and materials properties of new types of nanocomposite materials that are not only suitable for short-term packaging and disposable applications but also friendly to the ecosystem.

### Experimental Section

**Materials.** PLA with *D* content of 1.1–1.7% (supplied by Unitika Co. Ltd., Japan) was dried under vacuum at 60 °C and kept under dry nitrogen gas for 1 week prior to use. The organically modified synthetic fluorine mica (OMSFM) used in this study was supplied by CO-OP Chemicals Ltd., Japan, and was synthesized by replacing Na<sup>+</sup> in synthetic fluorine mica (SFM) (original thickness of ~1 nm and average length of 200–300 nm) of a cation exchange capacity (CEC) of 120 mequiv/100 g with *N*-(coco alkyl)-*N,N*-[bis(2-hydroxyethyl)]-*N*-methylammonium cation by ion exchange reaction.

**Nanocomposites Preparation.** For nanocomposites preparation, OMSFM (powder form) and PLA (pellets form) were first dry-mixed by shaking them in a bag. The mixture was then melt-extruded by using a twin-screw extruder (PCM-30, Ikegai Machinery Co.) operated at 210 °C<sup>20</sup> (screw speed = 100 rpm, feed rate = 120 g/min) to yield nanocomposite strands. Henceforth, the product nanocomposites were abbreviated as PLACNs. PLACNs prepared with three different amounts of OMSFM of 4, 7, and 10 wt % were correspondingly abbreviated as PLACN4, PLACN7, and PLACN10, respectively. The strands were pelletized and dried under vacuum at 60 °C for 48 h to remove water.

The dried PLACNs pellets were then converted into sheets with a thickness of 0.7–2 mm by pressing with ~1.5 MPa at 190 °C for 3 min. The molded sheets were then quickly quenched between glass plates and then annealed at 110 °C for 1.5 h to crystallize isothermally before being subjected to wide-angle X-ray diffraction (WAXD), transmission electron micrograph (TEM), and dynamic mechanical properties measurements.

### Characterization Methods

**WAXD.** WAXD analyses were performed for the OMSFM powder and various PLACNs using an MXlabo X-ray diffrac-

**Table 1. Characteristic Parameters of Neat PLA and Various PLACNs**

characteristic parameters	neat PLA	PLACN4	PLACN7	PLACN10
$M_w \times 10^{-3}$ (g·mol <sup>-1</sup> )	177	150	140	130
$M_w/M_n$	1.58	1.55	1.60	1.66
$T_g$ (°C)	60	56	55	55
$T_m$ (°C)	168.2	168.6	167.7	166.8
$T_c$ (°C)	127.2	99.4	97.6	96.5
$\chi_c$ (%)	36	40	46	43

tometer (MAC Science Co., generator of 3 kW, a graphite monochromator, Cu K $\alpha$  radiation (wavelength,  $\lambda = 0.154$  nm), operated at 40 kV/20 mA). The samples were scanned in fixed time (FT) mode with a counting time of 2 s under diffraction angle  $2\theta$  in the range of 1°–70°.

**TEM.** To clarify the nanoscale structure of various PLACNs, conventional TEM (JEM-200CX, JEOL) and high-resolution TEM (H-7100, Hitachi Co.) were also used, and both were operated at an accelerating voltage of 100 kV. The ultrathin sections of either crystallized pellets or sheets (perpendicular to the compression mold) with a thickness of ~100 nm were microtomed at –80 °C using a Reichert Ultra cut cryo-ultramicrotome without staining.

**Gel Permeation Chromatography (GPC).** Weight-average ( $M_w$ ) and number-average ( $M_n$ ) molecular weights of PLA (before and after nanocomposites preparation) were determined by means of GPC (LC-VP, Shimadzu Co.), using polystyrene standards for calibration and tetrahydrofuran (THF) as the carrier solvent at 40 °C with a flow rate of 0.5 mL/min. For the GPC measurements first PLA or PLACNs were dissolved in CHCl<sub>3</sub> and then diluted with THF.

GPC results of PLA in the pure state or in OMLS-filled systems are presented in Table 1. As anticipated, the incorporation of OMSFM resulted in a reduction in the molecular weight of the PLA matrix. Decreased molecular weights of nanocomposites may be explained by either the shear mixing of PLA and OMSFM or the presence of hydroxy groups in modified salt, both resulting in a certain degree of hydrolysis of PLA matrix at high temperature.

**Differential Scanning Calorimeter (DSC).** The glass transition ( $T_g$ ), melting ( $T_m$ ), and crystallization ( $T_c$ ) temperatures and degree of crystallinity ( $\chi_c$ ) of neat PLA and various PLACNs were determined by a temperature-modulated DSC (TMDSC) (MDSC, TA2920, TA instruments), operated at a heating rate of 5 °C/min with a heating/cooling cycle of the modulation period of 60 s and an amplitude of  $\pm 0.769$  °C. For the measurement of  $\chi_c$  prior to DSC analysis, the extra heat absorbed by the crystallites formed during heating had to be subtracted from the total endothermic heat flow due to the melting of the whole crystallites. This can be done according to the principles and procedures described in our previous paper.<sup>21</sup> By considering the melting enthalpy of 100% crystalline poly(L-lactide) as 93 J/g,<sup>22</sup> we have estimated the value of the  $\chi_c$  of neat PLA and various PLACNs, and these values are presented in Table 1.

**Light Scattering (LS) and Polar Optical Micrographic (POM) Observations.** To investigate the crystallite texture, the neat PLA and PLACN4 samples were subjected to LS experiments under Hv scattering mode with the radiation of a polarized He–Ne laser of 632.8-nm wavelengths. The details of the LS measurement were described in our previous paper.<sup>23</sup>

We also observed crystallite growth behavior of neat PLA and PLACN4 by means of POM. Dried pellets were sandwiched between two glass slides, placed on a laboratory hot plate at 190 °C for 60 s to obtain a thin film ~30  $\mu$ m in thickness. The molten film was then quickly quenched to the desired temperature (110 °C) by putting it on a thermostated

(16) Chen, J.-S.; Poliks, M. D.; Ober, C. K.; Zhang, Y.; Wiesner, U.; Giannelis, E. P. *Polymer* **2002**, *43*, 4895.

(17) Sinha Ray, S.; Maiti, P.; Okamoto, M.; Yamada, K.; Ueda, K. *Macromolecules* **2002**, *35*, 3104.

(18) Sinha Ray, S.; Okamoto, K.; Yamada, K.; Okamoto, M. *Nano Lett.* **2002**, *2*, 423.

(19) Sinha Ray, S.; Yamada, K.; Okamoto, M.; Ueda, K. *Nano Lett.* **2002**, *2*, 1093. Sinha Ray, S.; Yamada, K.; Okamoto, M.; Ueda, K. *Polymer* **2003**, *44*, 857.

(20) We have checked the degradation of intercalated salt by using thermogravimetric (TG) analysis. Up to 210 °C, there is no degradation of intercalated salt.

(21) Nam, P. H.; Maiti, P.; Okamoto, M.; Kotaka, T.; Hasegawa, N.; Usuki, A. *Polymer* **2001**, *42*, 9633.

(22) Fischer, E. W.; Sterzel, H. J.; Wegner, G. *Kolloid Z. Z. Polym.* **1973**, *25*, 980.

(23) Okamoto, M.; Kubo, H.; Kotaka, T. *Macromolecules* **1998**, *31*, 4223.

hot stage (Linkam RTVMS, Linkam Scientific Instruments, Ltd.) mounted on a POM (Nikon OPTIPHOTO2-POL). After complete crystallization, the nature of crystallite growth was observed using POM.

**Dynamic Mechanical Analysis (DMA).** Dynamic mechanical properties of the neat PLA and various PLACNs were measured with a Reometrics Dynamic Analyzer (RDIII) in the tension-torsion mode. The temperature dependence of a dynamic storage modulus ( $G'$ ), loss modulus ( $G''$ ), and  $\tan \delta$  of neat PLA and various PLACNs were conducted at a constant frequency ( $\omega$ ) of 6.28 rad/s with the strain amplitude of 0.05% and in the temperature range of  $-20$  to  $160$  °C with a heating rate of  $2$  °C/min.

**Flexural Properties and Heat Distortion Temperature (HDT).** The dried neat PLA and various PLACNs pellets were injection-molded using an injection machine (IS-80G, Toshiba Machinery Co.) operated at  $190$  °C with a mold temperature of  $30$  °C. Flexural modulus and strength of the injection-molded specimens (thickness  $\sim 3.2$  mm, annealed at  $120$  °C for 30 min) were measured according to the ASTM D-790 method (Model 2020, Intesco Co.) with a strain rate of  $2$  mm/min at room temperature ( $\sim 25$  °C). The HDT tests of neat PLA and various PLACNs were conducted using crystallized injection-molded samples (HDT Tester, Toyoseiki Co.) according to the ASTM D-648 method with a heating rate of  $2$  °C/min. We also conducted load dependence of HDT of neat PLA and PLACN7 using the same procedure.

**Measurement of O<sub>2</sub> Gas Transmission Rates.** Oxygen gas transmission rates of neat PLA and various PLACNs were measured at  $20$  °C and 90% relative humidity by the ASTM D-1434 differential pressure method (GTR-30XAU, Yanaco Co.). Test samples were prepared by compression molding (thickness  $\sim 300$  mm) and melt-quenched amorphous samples were used for this measurement.

**Biodegradability.** The biodegradability of neat PLA and PLACN4 were studied on a homemade compost instrument at  $58 \pm 2$  °C. The used compost was prepared from bean-curd refuse, food waste, and cattle feces. The degree of biodegradation, that is, CO<sub>2</sub> evolution, was measured directly by means of an attached FT-IR spectrometer (Horiba FT-730). The test specimens were crystallized neat PLA and PLACN4 pellets.

## Results and Discussion

**Nanocomposites Structure.** The structure of the nanocomposites in the nanometer range has typically been established using WAXD patterns and TEM observations. WAXD allows direct evidence of the intercalation of the polymer chains into the silicate galleries, whereas TEM offers a qualitative understanding of the internal structure through direct visualization. Here, first we combine WAXD and CTEM to examine the structure of various PLACNs, and then using CTEM and HRTEM, we examine the final structure of these PLACNs. Figure 1 represents the WAXD patterns of pure OMSFM powder and various PLACNs in the range of  $2\theta = 1^\circ$ – $10^\circ$ . The mean interlayer spacing of the (001) plane ( $d_{001}$ ) for the OMSFM powder obtained by WAXD measurements is  $2.08$  nm ( $2\theta = 4.20^\circ$ ). In the case of PLACN4, a sharp peak is observed at  $2\theta = 2.86^\circ$  ( $=3.09$  nm), corresponding to the (001) plane of the stacked and intercalated silicate layers dispersed in the PLA matrix, accompanied by the appearance of a small peak at  $5.65^\circ$ . After calculation, it was confirmed that this peak was due to the (002) plane ( $d_{002}$ ) of the dispersed OMSFM in the PLA matrix. With increasing OMSFM content, these peaks become stronger and shift toward the higher diffraction angle at  $2\theta = 3.13^\circ$  and  $5.9^\circ$ , respectively, for PLACN10. These behaviors are due to a decrease in percentage of polymer chains to be intercalated and

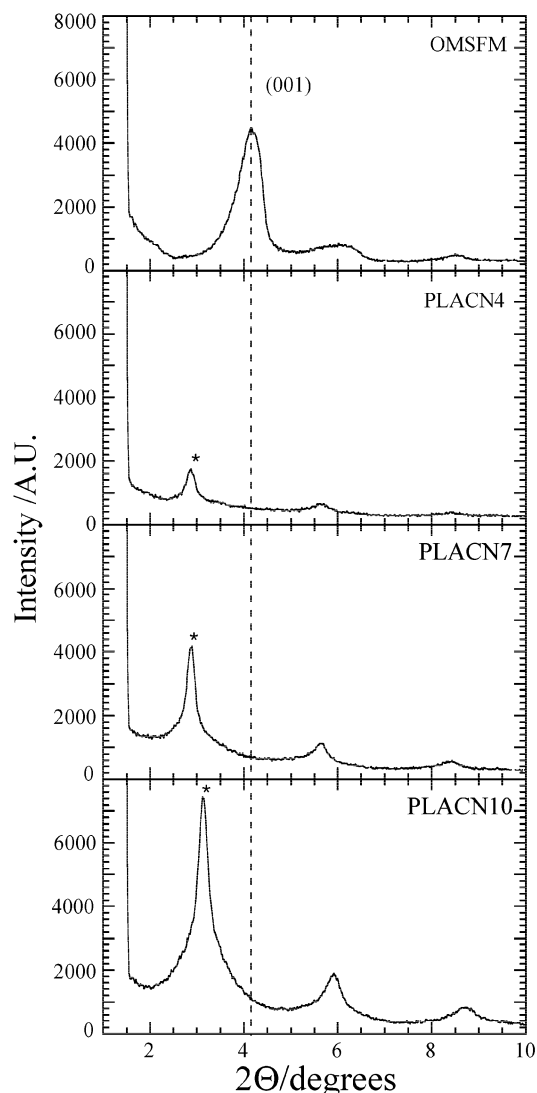


**Figure 1.** WAXD patterns of OMSFM powder and various PLACNs. The dashed line indicates the location of the silicate (001) reflection of OMSFM. The asterisks indicate the (001) peak for OMSFM dispersed in a PLA matrix.

increase stacking of the intercalated silicate layers with increasing OMSFM content. The width of the WAXD peak,  $\beta$  (measured by the full-width at half-maximum), is inversely proportional to the coherence length of scattering entities,  $D$ , and therefore reflects the coherent order of the silicate layers.<sup>24,25</sup> Since the width of the basal spacing of OMSFM decreased sharply after nanocomposite preparation with PLA, therefore, the coherence of the intercalated OMSFM layers much higher than that of un-intercalated OMSFM layers and increases with increasing OMSFM content. Thus, we can make conclusions on the basis of WAXD analysis that PLA chains were intercalated, have a strong effect on the layer structure of OMSFM, and sharply change the coherence length of the intercalated silicate crystallites with increasing OMSFM content.<sup>26</sup>

(24)  $D = (\lambda k) / (\beta \cos \theta)$ , where  $k$  is a constant and generally equal to 0.9,  $\lambda = 0.154$  nm, and  $\theta$  is the WAXD peak position.

(25) Drits, V. A.; Tchoubar, C. *X-ray Diffraction by Disordered Lamellar Structures*; Springer-Verlag: New York, 1990; 21–22. Cullity, B. D. *Principles of X-ray diffraction*; Addison-Wesley: Reading, MA, 1978.

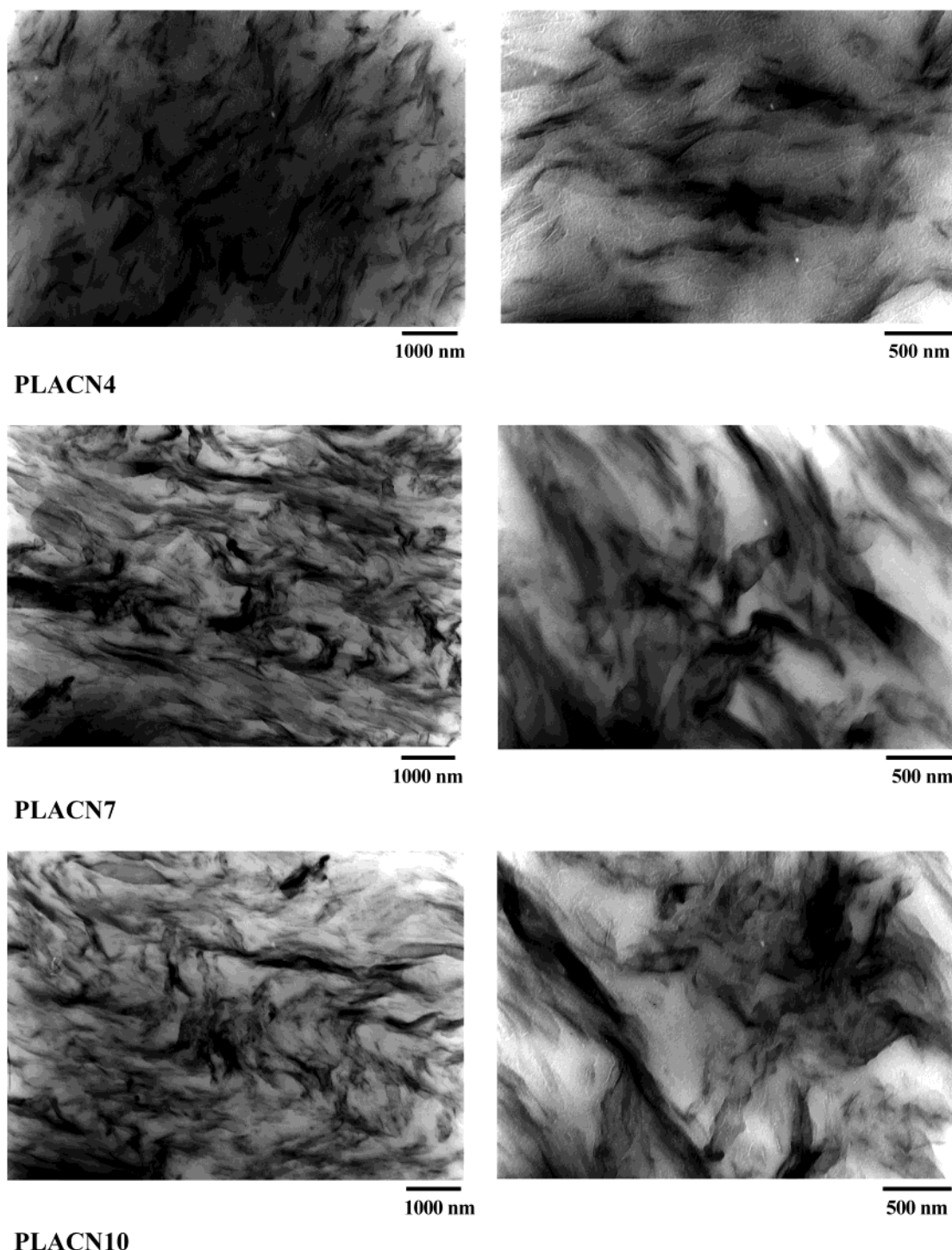


**Figure 2.** Bright field TEM (conventional) observations of various crystallized PLACNs pellets.

Figure 2 shows the CTEM images of various PLACNs pellets of two different magnifications in which dark entities are the cross section of the intercalated OMSFM layers and bright areas are the matrix.<sup>27</sup> From the TEM images we observed stacked and flocculated silicate layers, which are nicely distributed in the PLA matrix.

**Thermal Properties and Crystallite Morphology.** Figure 3a shows DSC traces for the melt-quenched amorphous samples of neat PLA and various PLACNs.

These data are obtained from the first run and during the heating process. Samples were prepared by using a hot press. Neat PLA and various PLACNs pellets were melted at 190 °C, held for 3 min at the same temperature under ~1.5 MPa pressure, and then quickly

(26) Sinha Ray, S.; Yamada, K.; Okamoto, M.; Fujimoto, Y.; Ogami, A.; Ueda, K. *Polymer*, submitted. Sinha Ray, S.; Okamoto, K.; Okamoto, M. *Macromolecules* **2003**, in press.

(27) Since the silicate layers are comprised of heavier elements (Al, Si, O) than the interlayer and surrounding matrix (C, H, N, etc.), they appear darker in bright field images. Klimentidis, R. E.; Mackinnon, I. D. R. *Clays Clay Miner.* **1986**, *34*, 155. Grim, R. E. *Clay Mineralogy*; McGraw-Hill: New York, 1953. Pinnavaia, T. J. In *Chemical Physics of Intercalation*; Legrand, A. P., Flandrois, S., Eds.; Plenum: New York, 1987. Güven, N. In *Hydrous Phyllosilicates*; Bailey, S. W., Ed.; Mineralogical Society of America: Washington, DC, 1988; Reviews in Mineralogy.

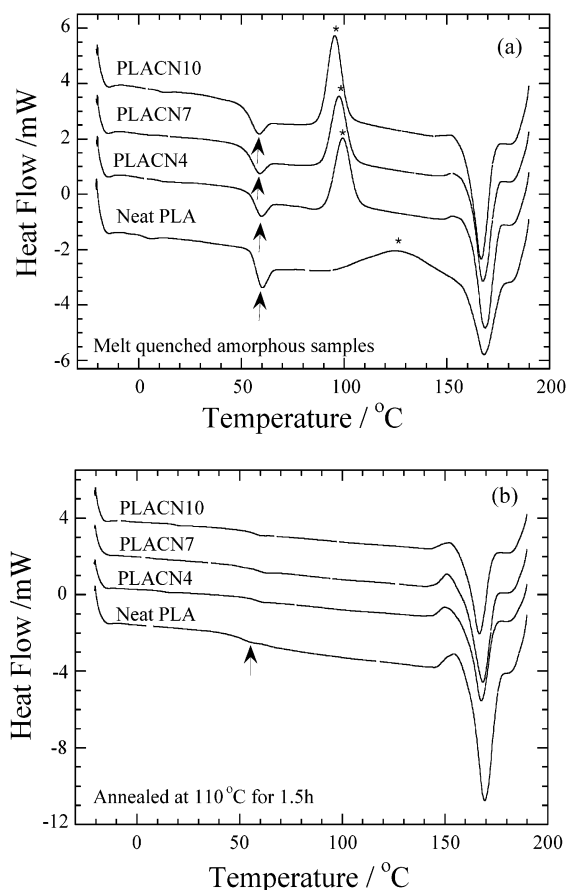


**Figure 3.** (a) DSC scans of the melt-quenched amorphous samples of neat PLA and various PLACNs. (b) DSC scans of the annealed samples of neat PLA and various PLACNs.

quenched between glass plates. From Figure 3a, we can see an endothermic peak for all samples in the temperature range of 55–60 °C. The temperature according to the endothermic peak for each sample is considered to be  $T_g$  of PLA. For all samples at  $T_g$  there is a steplike change, which is due to enthalpy relaxation.<sup>28</sup>

On the other hand, all samples show an exothermic peak and that can be correlated to the crystallization of PLA in every sample; the corresponding temperature is known as the crystallization temperature,  $T_c$ . In the case of PLACNs this peak is sharper and appeared at lower temperature than that of neat PLA and gradually shifted toward a lower temperature with increasing OMSFM content (Table 1). Therefore, the OMSFM seems to enhance the rate of crystallization of PLA. It should be noted here that  $T_c$  does depend on the OMSFM content but not strongly. This behavior suggests that a small amount of OMSFM is enough to serve as a nucleating agent for crystallization. However, all samples do not show the exothermic peak when annealed at 110 °C for 1.5 h before being subjected to DSC analyses (Figure 3b). This result indicates PLA matrixes were crystallized during heat treatment at 110 °C for 1.5 h.<sup>29</sup> A systematic DSC study of both samples (either annealed or not) shows that the  $T_g$  signal of neat PLA gradually weakens with increasing OMSFM content.

(28) Wunderlich, B. *Macromolecular Physics*; Academic Press: New York, 1976; Vol. 2, p. 363.

(29) Eling, B.; Gogolewski, S.; Pennings, A. J. *Polymer* **1977**, *23*, 1587.

This behavior suggests that OMSFM layers affect all polymers and there is a very small amount of bulklike PLA present to manifest itself through the thermal transition.

POM photographs of neat PLA and PLACN4 are presented in Figure 4. Both samples were crystallized at 110 °C beforehand. Neat PLA exhibits well-defined large crystallite morphology, whereas the size of the PLACN4 crystallites is significantly smaller. This observation indicates that the surface of dispersed OMSFM has a very strong effect on PLA crystallization.

This behavior is more clearly seen in LS patterns, where for PLACN4, a large smeared four-leaf-clover pattern is observed compared to the crystallized neat PLA, indicating the formation of a large number of less well-organized crystallite. From LS patterns, the number of heterogeneous nuclei  $N$  can be estimated from a rough approximation. That is, all the crystallites are of identical size. The primary average nucleation density of the crystallites, that is,  $N$ , is given by<sup>30</sup>

$$N = (3/4\pi)(D_m/2)^{-3}$$

where  $D_m$  is the average maximum diameter of the crystallite, that is, the attainable diameter before impingement. The calculated values of  $N$  at 110 °C were  $7 \times 10^{-4}$  for PLACN4 and  $8 \times 10^{-5}$  for neat PLA, respectively. This behavior indicates that the surface of the dispersed OMSFM layers acts as a nucleating agent for PLA crystallization, which is evident from the increase in the number of density of nuclei causing smaller crystallites formation.<sup>30</sup> Since these are exfoliated systems, therefore, we believe intercalation of polymer chains in extended conformations has almost no effect on crystallization. However, in the case of ordered intercalated PLA/C<sub>18</sub>-mnt nanocomposites, it has a strong effect on crystallization.<sup>31</sup> So our investigation explores the role of OMSFM as a nucleating agent for PLA crystallization. Such discussion is beyond the objective of this paper, and we will report it separately.<sup>31</sup>

**Dynamic Mechanical Analysis.** DMA measures the response of a given material to an oscillatory deformation (here in tension-torsion mode) as a function of the temperature. DMA results are expressed by three main parameters: (a) the storage modulus ( $G'$ ) corresponding to the elastic response to the deformation; (b) the loss modulus ( $G''$ ), corresponding to the plastic response to the deformation; and (c)  $\tan \delta$ , that is, the ( $G''/G'$ ) ratio, useful for determining the occurrence of molecular mobility transitions such as the glass transition temperature.

Here, DMA analysis has been studied to track the temperature dependence of  $G'$ ,  $G''$ , and  $\tan \delta$  of neat PLA upon the PLACNs formation with OMSFM. Figure 5 shows the temperature dependence of  $G'$ ,  $G''$ , and  $\tan \delta$  for neat PLA and corresponding PLACNs. For all PLACNs, a significant enhancement of  $G'$  can be seen in the investigated temperature range, indicating intercalated PLACNs have a strong influence on the elastic properties of the PLA matrix.

(30) Maiti, P.; Nam, P. H.; Okamoto, M.; Usuki, A.; Hasegawa, N. *Macromolecules* **2002**, *35*, 2042 and references therein.

(31) Sinha Ray, S.; Okamoto, M.; Yamada, K.; Ueda, K., in preparation.

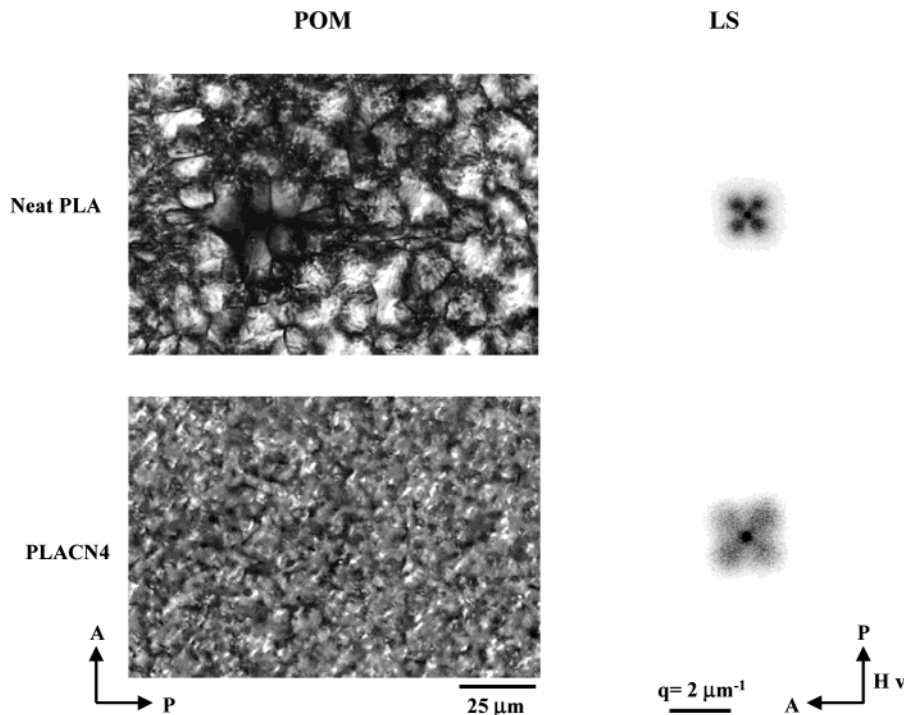


**Figure 4.** Polarized optical micrographs and the corresponding Hv-light scattering patterns for neat PLA and PLACN4 isothermally crystallized at 110 °C for 1.5 h.

Below  $T_g$ , the enhancement of  $G'$  is clear in the intercalated PLACNs. In the temperature range of  $-20$  to  $25$  °C, the increases in  $G'$  are 23% for PLACN4, 62% for PLACN7, and 125% for PLACN10 as compared to that of the neat PLA (see Figure 5). Furthermore, in the temperature range of  $80$  to  $145$  °C all three PLACNs exhibit much higher enhancement of  $G'$  as compared to that of neat PLA. This is due to both mechanical reinforcement by clay particles and extended intercalation at high temperature.<sup>17,32</sup> Above  $T_g$ , when materials become soft, reinforcement effect of the clay particles becomes prominent, due to the restricted movement of the polymer chains, and hence strong enhancement of modulus appeared.<sup>15</sup> In Table 2, we summarized the  $G'$  values of neat PLA and various PLACNs in different temperature ranges. At room temperature ( $25$  °C), PLACN7 and PLACN10 exhibited higher increments in  $G'$  of 66% and 129%, respectively, as compared to that of neat PLA, whereas PLACN4 showed only a 26% increment.

On the other hand, above  $T_g$  the enhancement of  $G''$  is significant in the intercalated PLACNs compared to that below  $T_g$ , indicating plastic response to the deformation is prominent in the presence of OMSFM when the material becomes soft. However, the presence of OMSFM does not lead to a significant shift and broadening of the  $\tan \delta$  curves for all PLACNs compared to that of neat PLA. This behavior has been ascribed to the restricted segmental motions in the organic–inorganic interface neighborhood of intercalated PLACNs.<sup>17</sup>

**Flexural Properties and HDT.** In Table 3, we report the flexural modulus and strength of neat PLA and various PLACNs measured at  $25$  °C. There is a

significant increase in flexural modulus for PLACN4 of 26% compared to that of neat PLA followed by a low value of modulus in the case of PLACN7 and a maximum of a 50% increase in the case of PLACN10. On the other hand, flexural strength remarkably increases with PLACN4, further increases with PLACN7, and then sharply decreases in the case of PLACN10. This behavior may be due to high OMSFM content, which leads to a brittleness of PLACN10. Therefore, we may control the flexural strength by increasing or decreasing OMSFM content, and incorporation of OMSFM of around 7 wt % is the optimum to achieve the high value of flexural strength.

The nanodispersion of OMSFM in neat PLA also promotes a higher HDT. We examined the HDT of neat PLA and various PLACNs with different load conditions. As seen in Figure 6a, in the case of PLACN4, there is a marked increase in HDT with intermediate load of 0.98 MPa, from  $76$  °C for the neat PLA to  $93.2$  °C for PLACN4. The value of HDT gradually increases with increasing OMSFM content, and in the case of PLACN10, the value increases up to  $115$  °C. This increase in HDT of neat PLA after nanocomposites preparation is a very important property improvement, not only from the industrial point of view but also in molecular level control of some properties on the silicate layers, that is, crystallization through interfacial interaction between PLA molecules and  $\text{SiO}_4$  tetrahedral layers.

On the other hand, imposed load dependence on HDT is clearly observed in the case of PLACNs. Figure 6b shows the typical load dependence in the case of PLACN7. From Figure 6b, we can see in the low load region there is a significant improvement in HDT in the case of PLACN7 compared to that of neat PLA, and with increasing load this improvement gradually decreases. In the case of nanocomposites with high load (1.81 MPa

(32) Sinha Ray, S.; Okamoto, K.; Okamoto, M. *J. Nanosci. Nanotechnol.* **2002**, *2*, 471.

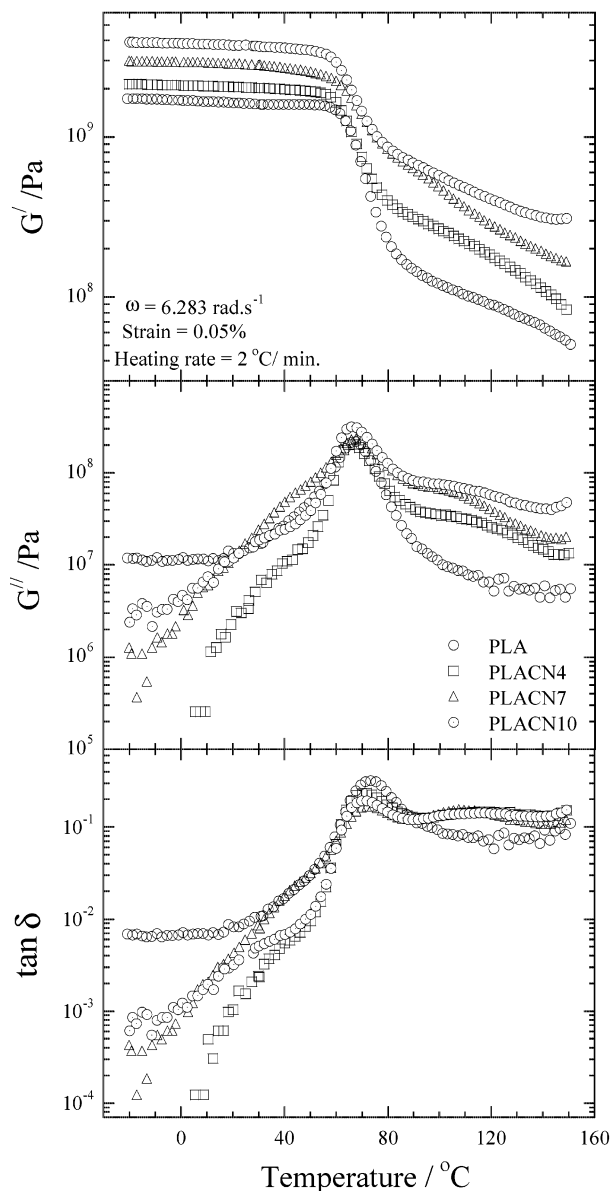


**Figure 5.** Temperature dependence of storage modulus ( $G'$ ), loss modulus ( $G''$ ), and their ratio,  $\tan \delta$ , for neat PLA and various PLACNs.

**Table 2.**  $G'$  Values of Neat PLA and Various PLACNs at Different Temperatures

samples	$G'$ (GPa)					
	-20 °C	0 °C	25 °C	50 °C	100 °C	150 °C
neat PLA	1.73	1.69	1.61	1.59	0.12	0.05
PLACN4	2.12	2.09	2.03	1.91	0.26	0.08
PLACN7	2.80	2.76	2.67	2.36	0.43	0.24
PLACN10	3.90	3.83	3.69	3.46	0.56	0.31

**Table 3.** Flexural Properties of Neat PLA and Various PLACNs

flexural properties	neat PLA	PLACN4	PLACN7	PLACN10
modulus/GPa at 25 °C	4.84	6.11	5.55	7.25
strength/MPa at 25 °C	86	94	101	78

or more), it is very difficult to achieve high HDT improvement without strong interaction between polymer matrix and layered silicates.<sup>33</sup> For all PLACNs studied here, the values of  $T_m$  (cf. Table 1) do not change significantly as compared to that of neat PLA. Further-

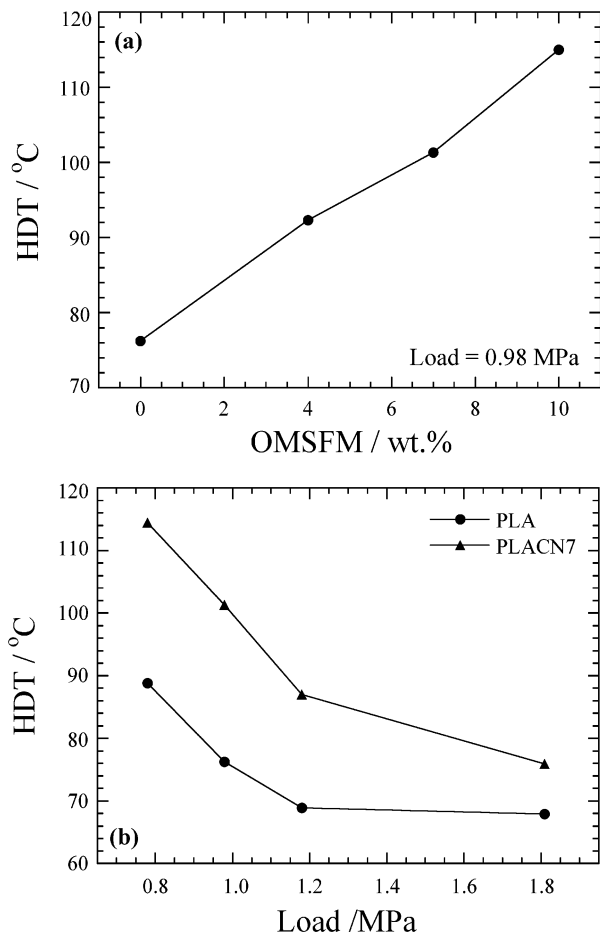


**Figure 6.** (a) Organoclay (OMSFM) (wt %) dependence of HDT of neat PLA and various PLACNs. (b) Load dependence of HDT of neat PLA and PLACN7.

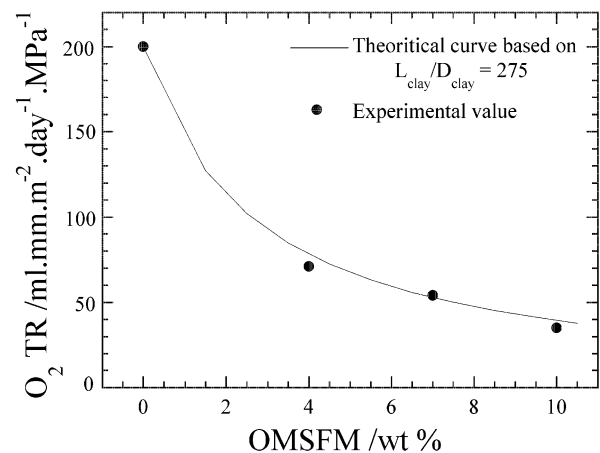


**Figure 7.** Oxygen gas permeability of neat PLA and various PLACNs as a function of OMSFM content (wt %) at 20 °C and 90% relative humidity. The filled circles represent the experimental data. Theoretical fits based on the Nelson tortuosity model.

more, in WAXD analyses of crystallized samples up to  $2\theta = 70^\circ$ , we do not observe significant shifting or formation of new peaks in the crystallized PLACN samples. So the improvement of HDT with intermediate load (0.98 MPa) originates from the better mechanical

(33) Manias, E.; Touny, A.; Wu, L.; Strawhecker, K.; Lu, B.; Chung, T. C. *Chem. Mater.* **2001**, *13*, 3516.

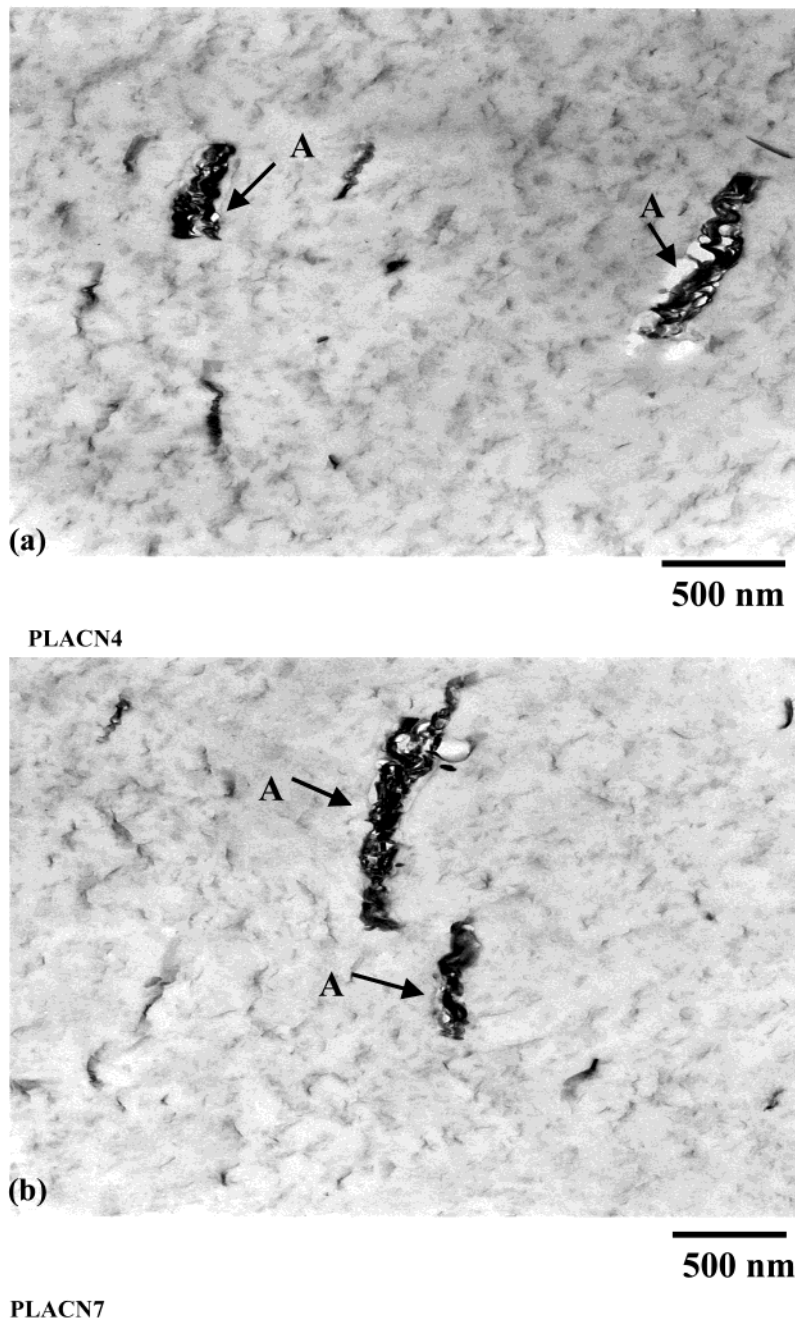


**Figure 8.** High-resolution bright field TEM images of (a) PLACN4 and (b) PLACN7 compress molding crystallized sheets.

stability of the PLACNs or is due to mechanical reinforcement by the dispersed clay particles, higher value of  $\chi_c$ , and intercalation.<sup>33</sup> This is qualitatively different from the behavior of Nylon-6/layered silicate nanocomposites; there is a strong interaction between layered silicates and the Nylon-6 matrix by forming hydrogen bonding.<sup>34</sup>

**O<sub>2</sub> Gas Permeability.** The gas barrier properties have been shown to improve dramatically upon exfoliation of clay platelets in a number of polymeric matrixes.<sup>35–39</sup> The mechanism for the improvement is

attributed to the increase in the tortuosity of the diffusive path for a penetrating molecule. Indeed, a simple tortuosity-based model<sup>40,41</sup> has been found to explain experimental trends satisfactorily.<sup>35–39</sup> The gas permeability of nanocomposites ( $P_{\text{PLACN}}$ ) is related to the permeability of the neat polymer ( $P_{\text{PLA}}$ ) and the volume fraction ( $\Phi_{\text{clay}}$ ) and width ( $D_{\text{clay}}$ ) of the clay as<sup>41</sup>

$$\frac{P_{\text{PLACN}}}{P_{\text{PLA}}} = \frac{1}{1 + (L_{\text{clay}}/2D_{\text{clay}})\phi_{\text{clay}}}$$

The above expression assumes that the sheets are

(34) Maiti, P.; Okamoto, M. *Macromol. Mater. Eng.*, submitted.  
 (35) Kojima, Y.; Usuki, A.; Kawasumi, M.; Okada, A.; Fukushima, Y.; Kurauchi, T. T.; Kamigaito, O. *J. Mater. Res.* **1993**, *8*, 1179. Kojima, Y.; Usuki, A.; Kawasumi, M.; Okada, A.; Kurauchi, T. T.; Kamigaito, O. *J. Polym. Sci., Part A: Polym. Chem.* **1993**, *31*, 983.  
 (36) Usuki, A.; Kawasumi, M.; Kojima, Y.; Okada, A.; Kurauchi, T.; Kamigaito, O. *J. Mater. Res.* **1993**, *8*, 1185.

(37) Yano, K.; Usuki, A.; Okada, A.; Kurauchi, T.; Kamigaito, O. *J. Polym. Sci., Part A: Polym. Chem.* **1993**, *8*, 1185.  
 (38) Messersmith, P. B.; Giannelis, E. P. *Chem. Mater.* **1994**, *6*, 1719.  
 (39) Xu, R.; Manias, E.; Snyder, A. J.; Runt, J. *Macromolecules* **2001**, *34*, 337.

placed such that the sheet plane is perpendicular to the diffusive pathway. The permeability of O<sub>2</sub> gas through the PLACNs films is shown in Figure 7. As seen from Figure 7, the permeability of O<sub>2</sub> gas through the PLACN films decreases significantly relative to that of the neat PLA film. Therefore, in terms of stacked intercalated structure (as observed with CTEM in Figure 2) we cannot explain high gas barrier properties of PLACNs relative to that of neat PLA.

To explain this behavior, we used a HRTEM instrument to examine the final structure of various PLACN sheets, which were used for gas permeability measurements. In (a) and (b) of Figure 8 we show the HRTEM bright-field images (edge of the samples sheet perpendicular to the compression mold) of PLACN4 and PLACN7, respectively. From the TEM images it becomes clear that there are some intercalated stacked ("A" in the TEM photographs) and disordered or exfoliated OMSFM layers coexisting in each nanocomposite structure. Only the stacked intercalated structures are responsible for very sharp WAXD reflection as observed in Figure 1, whereas disordered or exfoliated (which is the maximum part as observed from TEM photographs, Figure 8). OMSFM structures have no periodic stacking and thus remain WAXD silent. We believe this type of mixed intercalated/exfoliated structure originates from the chemical and size inhomogeneities of the OMSFM layers. Typically, the large-in-lateral-size OMSFM layers create a stacked intercalated structure, whereas the smaller layers tend to exfoliate.

In Figure 7, we draw a theoretical curve considering  $L_{\text{clay}} = 275$  nm (calculated from TEM photographs in Figure 8, the actual value is  $275 \pm 25$  nm but we used the average value for theoretical calculations) and  $D_{\text{clay}} = 1$  nm, and interestingly all experimental values (filled circles) are well-matched with the theoretical curve. That means, the maximum part of the OMSFM layers were exfoliated in the PLACNs structure and intercalated stacked layers have a very small effect on gas barrier properties.

This property improvement is very important for biodegradable polymers-based materials because these materials are very suitable for food-packaging industries.

**Biodegradability.** The most interesting and exciting aspect of this research is the enhancement of biodegradability of neat PLA after nanocomposites preparation with OMSFM. Despite the considerable amount of reports concerning the enzymatic degradation of PLA<sup>42</sup> and various PLA blend,<sup>43</sup> there remains very little information regarding the compost degradability of PLA.<sup>1,5,44</sup> For the biodegradability study we choose PLACN4 as a representative nanocomposite. For the neat PLA and PLACN4, respirometric tests were carried

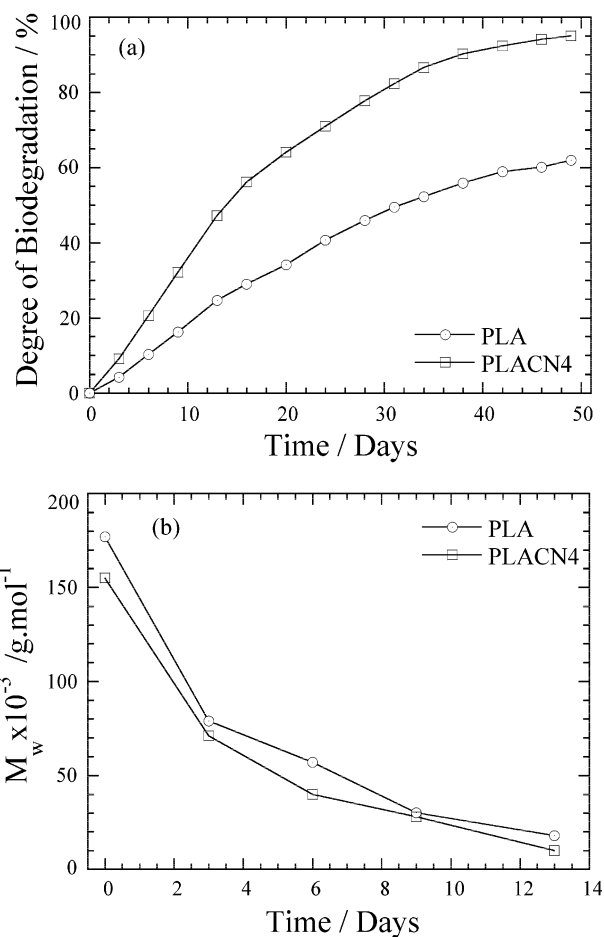


**Figure 9.** (a) Degree of biodegradation (i.e., CO<sub>2</sub> evolution) of neat PLA and PLACN4 under compost at  $58 \pm 2$  °C. (b) Time dependence change of matrix  $M_w$  of neat PLA and PLACN4 under compost at  $58 \pm 2$  °C.

out to study PLA-matrix degradation in a compost environment at  $58 \pm 2$  °C.<sup>1,5,44,45</sup> Unlike weight loss, which reflects the structural changes in the test sample, CO<sub>2</sub> evolution provides an indicator of the ultimate biodegradability, that is, mineralization of the test sample samples. In Figure 9a we report the time-dependence biodegradation (i.e., CO<sub>2</sub> evolution) of neat PLA and PLACN4. These data clearly indicate that the biodegradability of PLA component in PLACN4 was enhanced significantly after incorporation of OMSFM filler. The compost degradation of PLA occurs by a two-step process. During the initial phases of degradation, the high-molecular-weight PLA chains hydrolyze to lower molecular weights oligomers. This reaction can be accelerated by acids or bases and is also affected by both temperature and moisture. Fragmentation of the plastic occurs during this step at a point where the  $M_n$  decreases to less than about 40 000. At about this same  $M_n$ , micro-organisms in the compost environment continue the degradation process by converting these lower molecular components to CO<sub>2</sub>, H<sub>2</sub>O, and humus.<sup>44</sup> Therefore, any factor that increases the hydrolysis tendency of a PLA matrix ultimately control the degradation of PLA.

(45) We intentionally chose this temperature because we want to know any difference in rate of biodegradation between neat PLA and PLACN4 since the rate of biodegradation of neat PLA is very slow at ambient temperature.

(40) Beall, G. W. In *Polymer-Clay Nanocomposites*; Pinnavaia T. J., Beall, G. W., Eds.; Wiley: New York, 2001; p 267.

(41) Nielsen, L. J. *Macromol. Sci. Chem.* **1967**, *A1*(5), 929.

(42) Reeve, M. S.; McCarthy, S. P.; Downey, M. J.; Gross, R. A. *Macromolecules* **1994**, *27*, 825 and references therein. Iwata, T.; Doi, Y. *Macromolecules* **1998**, *31*, 2461.

(43) Hakkarainen, M.; Karlsson, S.; Albertsson, A.-C. *Polymer* **2000**, *41*, 2331.

(44) Narayan, R. Degradation of Polymeric Materials. In *Science and Engineering of Composting, Environmental, Microbiological and Utilization Aspects*; Hoitink, H. A., Keener, H. N., Eds.; OARDC: Columbus, OH, 1993.

It is well-known that PLA of relatively lower molecular weights may show higher rates of enzymatic degradation because of, for example, the high concentration of accessible chain end groups.<sup>46,47</sup> However, in this case the rate of molecular weight change of neat PLA and PLA in PLACN4 is almost the same (Figure 9b). So the initial molecular weight is not a main factor here for controlling the biodegradability of PLACN4. Another factor that controls the biodegradability of PLA is the  $\chi_c$  value because the amorphous phase is easy to degrade compared to the crystal phase. In Table 1, we show the  $\chi_c$  value of neat PLA is lower than that of PLACN4.

These data indicate that the incorporation of OMSFM in the nanocomposites resulted in a different mode of attack on the PLA component of the test samples. Since PLA is an aliphatic polyester, it is conceivable that incorporation of the OMSFM resulted in a different mode of disruption of some of the ester linkages due to the presence of hydroxy groups. Therefore, our research explores the role of OMSFM as a nanoscale filler for the enhancement of biodegradability of PLA.

### Conclusions

We have successfully prepared biodegradable PLA/OMSFM nanocomposites by simple melt extrusion of

(46) Kawai, F. *CRC Crit. Rev. Biotechnol.* **1987**, 6 (3), 273.

(47) Taino, T.; Fukui, T.; Shirakura, Y.; Saito, T.; Tomita, K.; Kaiho, T.; Masamune, S. *Eur. J. Biochem.* **1982**, 124, 71.

PLA and OMSFM, wherein silicate layers of OMSFM are intercalated, exfoliated, and a mixture of both. All the nanocomposites exhibited dramatic improvement in various materials properties as compared to those of neat PLA. These improvements include rate of crystallization, mechanical and flexural properties, heat distortion temperature, and O<sub>2</sub> gas permeability, with a simultaneous improvement in biodegradability of neat PLA. These are entirely new types of materials derived from plant and nature (OMSFM). When disposed of in compost, these are safely decomposed into CO<sub>2</sub> and H<sub>2</sub>O through the activity of micro-organisms. The CO<sub>2</sub> will become corn or sugarcane again through plant photosynthesis. Thus, these materials hold very strong future promise for potential applications as high-performance biodegradable materials.

**Acknowledgment.** Thanks are due to the Japan Society for the Promotion of Science (JSPS) for the award of a JSPS Postdoctoral Fellowship (ID No. P02152) and a research grant to S. Sinha Ray. The authors would also like to thank Mr. Y. Fujimoto for his help with LS and POM experiments. We also express our appreciation to the reviewers for their constructive and meticulous assessment of the manuscript.

CM020953R